COMMUNICATION
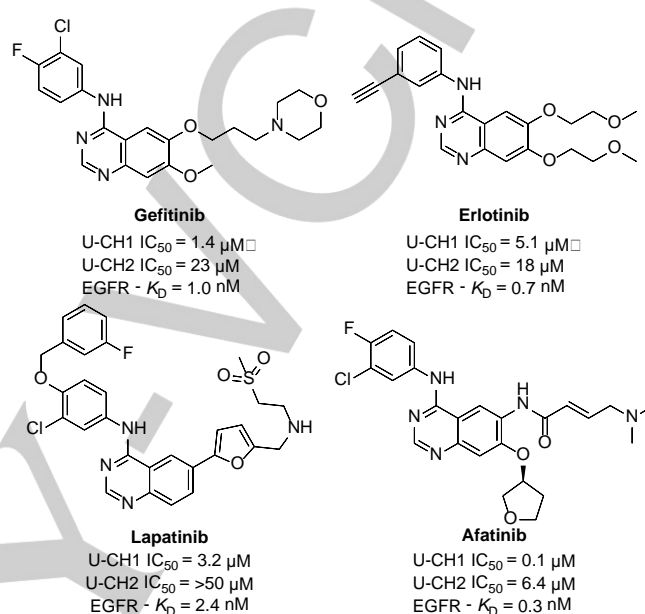
Targeting an EGFR water network using novel 4-anilinoquin(az)olines inhibitors for chordoma

Christopher R. M. Asquith,[a,b]* Kaitlyn A. Maffuid,[c] Tuomo Laitinen,[d] Chad D. Torrice,[c] Graham J. Tizzard,[e] Daniel J. Crona,[c,f] William J. Zuercher[b,f]*

Abstract: Quinoline- and quinazoline-based kinase inhibitors of the epidermal growth factor receptor (EGFR) have been used to target non-small cell lung cancer (NSCLC) and chordomas with varying amounts of success. We designed and prepared compounds to probe several key structural features including an interaction with Asp855 within the EGFR DGF motif and interactions with the active site water network. EGFR target engagement was then evaluated in a cellular assay, with the inhibitors then profiled in representative cellular models of NSCLC and chordomas. In addition to a structure activity relationship insight for EGFR inhibitor design with potent dimethoxy quin(az)oline identified (**1**, **4** & **7**). We also found a compound (**18**) that is the most potent inhibitor (IC_{50} = 310 nM) on the UCH-2 chordoma cell line to date.

Cancer is the second leading cause of death globally, and was responsible for an estimated 9.6 million deaths in 2018.[1] Kinases have been successfully utilized as drug targets for the past 30 years, with 49 kinase inhibitors approved by the FDA to date, mainly for cancer indications.[2] One target that has been intensely studied is epidermal growth factor receptor (EGFR). EGFR inhibitors including gefitinib and erlotinib provide significant clinical benefit in patients diagnosed with non-small cell lung cancer (NSCLC), while lapatinib was developed as a dual EGFR and HER2 inhibitor for the treatment of HER2-positive breast cancers (**Figure 1**).[3-5]

Therapeutic intervention in the EGFR pathway is not limited to NSCLC and breast cancer, along with a number of other cancers showing sensitivity to EGFR inhibitors.[6] These include chordomas, which are rare tumors that arise along the bones of the central nervous system and spine.[7] These tumors are a significant challenge to treat, and surgical resection is the current preferred course of treatment.[7-8] EGFR and its ligand EGF are highly expressed in chordomas, and copy number gains of EGFR occur in 40 % of chordomas. A number of EGFR inhibitors have been identified that are active in cellular models of chordoma (**Figure 1**), with afatinib currently in phase 2 clinical trials for the treatment of chordoma.[9-13]
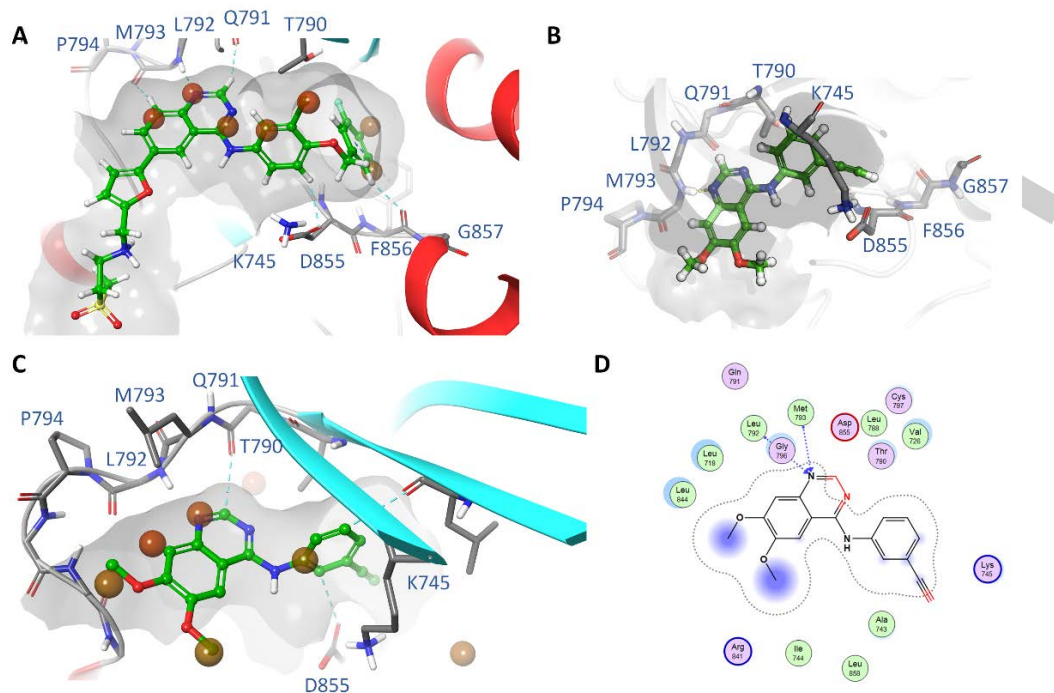
[a]   Dr. C. R. M. Asquith
        Department of Pharmacology, School of Medicine, University of North Carolina at Chapel Hill, NC 27599, (USA)
        E-mail: chris.asquith@unc.edu
[b]   Dr. C. R. M. Asquith, Prof. William J. Zuercher
        Structural Genomics Consortium, UNC Eshelman School of Pharmacy, University of North Carolina at Chapel Hill, Chapel Hill, NC 27599, (USA)
        E-mail: william.zuercher@unc.edu
[c]   Kaitlyn A. Maffuid, C. D. Torrice, Prof. D. J. Crona
        Division of Pharmacotherapy and Experimental Therapeutics, UNC Eshelman School of Pharmacy, University of North Carolina at Chapel Hill, Chapel Hill, NC 27599, (USA)
[d]   Prof. T. Laitinen
        School of Pharmacy, Faculty of Health Sciences, University of Eastern Finland, 70211 Kuopio, (Finland)
[e]   Dr. Graham J. Tizzard
        School of Chemistry, University of Southampton, Southampton, SO17 1BJ, (United Kingdom)
[f]   Prof. D. J. Crona, Prof. William J. Zuercher
        Lineberger Comprehensive Cancer Center, University of North Carolina at Chapel Hill, Chapel Hill, NC 27599, (USA)

Figure 1. Example structures of clinical EGFR quinazolines.

Gefitinib
U-CH1 IC_{50} = 1.4 µM
U-CH2 IC_{50} = 23 µM
EGFR - K_D = 1.0 nM

Erlotinib
U-CH1 IC_{50} = 5.1 µM
U-CH2 IC_{50} = 18 µM
EGFR - K_D = 0.7 nM

Lapatinib
U-CH1 IC_{50} = 3.2 µM
U-CH2 IC_{50} = >50 µM
EGFR - K_D = 2.4 nM

Afatinib
U-CH1 IC_{50} = 0.1 µM
U-CH2 IC_{50} = 6.4 µM
EGFR - K_D = 0.3 nM

Kinase inhibitors commonly have off-targets across the kinome that confound the ability to accurately define the mechanism of action that cause induction of phenotypes of interest.[14] The 4-anilino-quinoline and 4-anilino-quinazoline scaffolds have demonstrated a range of activity profiles across the kinome from highly selective to broadly promiscuous.[15-16] One recurring off-target of these scaffolds is cyclin G-associated kinase (GAK), which is frequently observed to bind 4-anilino-quinoline, quinazolines and 3-cyano-quinolines.[17] One example of a narrow spectrum kinome profile quinazoline is lapatinib, with only a handful of off-targets in addition to EGFR, HER2 and no GAK binding.[17]
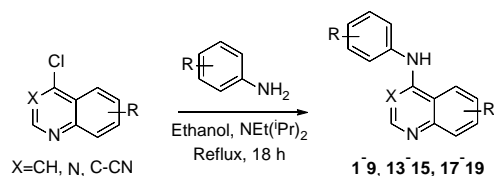
We docked lapatinib into the ATP binding site of EGFR and observed that the aniline portion was able to access a deeper lipophilic pocket, displacing 2 water molecules in the process (**Figure 2A**).[18-19] Inhibitors lacking an extended head-group were not able to access this pocket, including derivatives of erlotinib (**Figure 2B-D**). The methoxy groups also appeared to play an important role in binding by displacement of two additional water molecules at the solvent-exposed ATP binding site (**Figure 2C**) (PDB: 1XKK).[5] Employing the Schrödinger Maestro suite allowed us to explore the EGFR ATP-binding site properties with the 4-anilino-quin(az)oline scaffold (**Figure 2D**).[20]

Interested to explore these effects further, we designed and prepared several focused arrays of compounds to probe the structure activity relationships of the quinoline/quinazoline series. We synthesized a series of compounds (**1-9**, **13-15**, **17-19**) through nucleophilic aromatic displacement of commercially available 4-chloroquin(az)olines in excellent yields (58-85 %), consistent with previous reports (**Scheme 1**).[14-15,17]
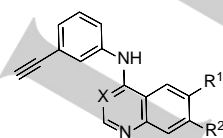
Figure 2. Examples of docked compounds in the EGFR ATP-binding domain (PDB: 1XKK). Red balls (A and C) are simulated waters with the ATP binding site.

X=CH, N, C-CN

Scheme 1. General synthetic procedure

These compounds were profiled in an EGFR cellular activity assay, two patient-derived chordoma cell lines (UCH-1 and UCH-2), a lung cancer cell line (A431), and a normal skin fibroblast line (WS1) (**Table 1** & **2**). The 6,7-dimethoxyquinolin-4-amine with the erlotinib 3-ethynylaniline (**1**) showed high potency in the cell-based EGFR phosphorylation assay (IC$_{50}$ = 270 nM), as previously reported.[13] The data from the two chordoma cell lines is also consistent with previous reports.[13] The A431 cells showed moderate activity at IC$_{50}$ = 1.4 µM and 3-fold weaker potency on WS1 normal fibroblast cell viability. The removal of either methoxy group to form the 6-methoxy (**2**) or 7-methoxy (**3**) yielded compounds with more than a 60-fold drop in EGFR in cell potency,

with respect to **1**. This structural modification also led to a loss of in cellular potency in both A431 and UCH-1 cell lines. In contrast, its potency in UCH-2 cells increased by more than 2-fold. However, the potency values of **2** and **3** were still in the low double digit micromolar range in UCH2 cells.

The switch from quinoline to quinazoline (**4**) showed a similar potency range to **1,** with slightly stronger potency in A431 cells. The removal of either methoxy (**5-6**) had no impact on cellular EGFR activity but did reduce activity in all 3 cancer cell lines, with no effect in WS1 cells. The 3-cyano quinoline hinge binder showed a marked drop off EGFR activity in cells. The 6,7-dimethoxy analog (**7**) showed similar potencies to the *mono*-methoxy quinazolines **5** and **6**. It was then surprising, that the removal of either methoxy (**8** and **9**) reduced the anti-proliferative effect seen in **7**; given that the EGFR cellular activity was near equipotent. This effect is likely due to the involvement of other targets.

With the results of the small focused series in hand, we then modified the aniline scaffold, with the aim of establishing an

Table 1. Results of a small series of compounds with varied hinge binding moieties (**1**-**9**).

Cmpd	R^1	R^2	X	EGFR^a IC$_{50}$ (µM)	A431	UCH-1	UCH-2	WS1
						IC$_{50}$ (µM)^b		
1	OMe	OMe	CH	0.27^c	1.4	0.54	42	4.6
2	OMe	H	CH	16	10	6.6	16	>100
3	H	OMe	CH	>20	3.4	9.4	17	>100
4	OMe	OMe	N	0.55^c	0.85	0.63	66	15
5	OMe	H	N	0.59	2.2	1.4	47	>100
6	H	OMe	N	0.53	8	1.9	1.2	>100
7	OMe	OMe	C-CN	1.8^c	1.7	4.1	36	>100
8	OMe	H	C-CN	3.5	>100	19.6	>100	>100
9	H	OMe	C-CN	1.1	44	4.1	40	>100

^{a}ProQinase In-cell assay (n=1), ^{b}(n=3), ^{c}Literature data reference 13

2
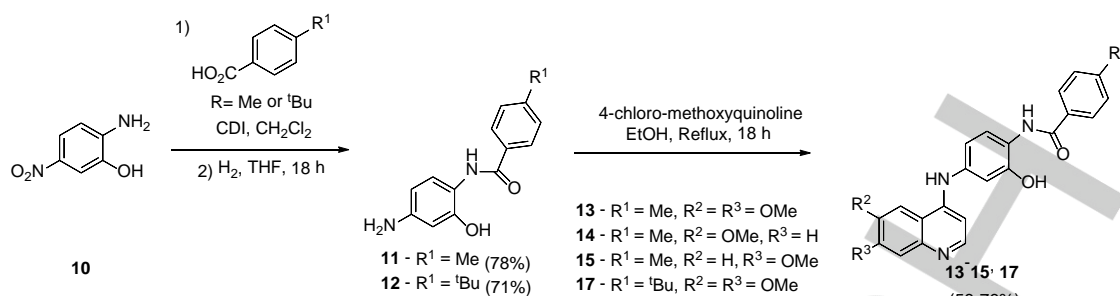
Scheme 2. Synthetic procedure for **13**-**15** and **17**
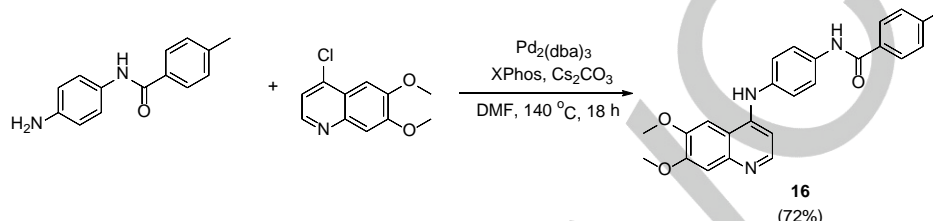
Scheme 3. Synthetic procedure for **16**

internal hydrogen bond, not only to form a pre-organized structure but also to engage in an interaction with Asp855 (**Figure 3**).
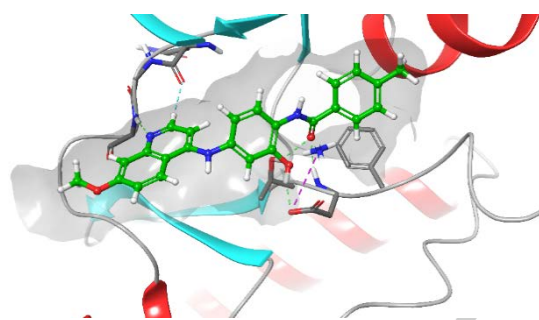

Figure 3. Docking of **15** into EGFR

In tandem, we looked at the water network in EGFR (**Figure 4**) and found that adding a methyl group to the pendent benzyl had the potential to increase potency by displacing a deep pocket water molecule.
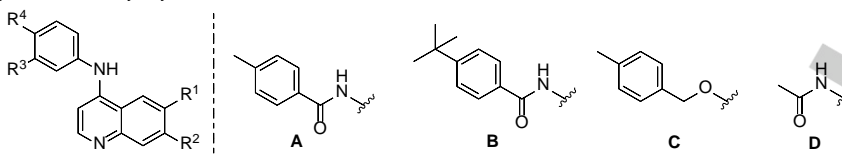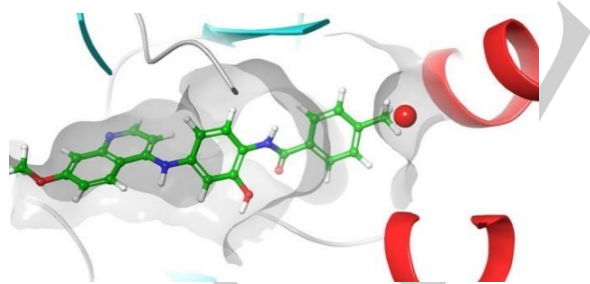

Figure 4. Docking pose of compound **15** superimposed with WaterMap simulation of EGFR (PDB:1XKK) showing displacement of high energy water.

We prepared several additional compounds (**13**-**18**) following a three-step protocol from commercially available 2-amino-5-nitrophenol (**10**) as a starting material. **10** was coupled with CDI to furnish an amide bond, followed by H_2 reduction to give intermediates **11** and **12** (**Scheme 2**). S_NAr reactions of intermediates **11** and **12** under reflux provided compounds **13**-**15** and **17** in good yields (58-76%).[15,17] The *des*-hydroxy compound (**16**) proved inaccessible *via* a nucleophilic aromatic displacement (even up to 150 °C, DMF, DIPEA, 18 h), and required Buchwald-Hartwig conditions (**Scheme 3**) to produce **16** in good overall yield (72 %).[15]

The 6,7-dimethoxyquinolin-4-amine with the lapatinib-derived hydroxy amide aniline (**13**) showed double digit micromolar potency in the cellular EGFR phosphorylation assay, moderate activity in A431 cells, and higher potency in UCH-1 and UCH-2 cells. Removal of either of the methoxy groups (**14** and **15**) led to an increase in activity in the chordoma cell lines with no change in their anti-proliferative effect within A431 cells. The activity profiles of **14** and **15** diverged from the results of monomethoxy compounds in the previous compound set (**1**-**9**).

Interestingly, our hypothesis of including the alcohol on the head-group proved to be pivotal for activity: removal of the alcohol (**16**) led to diminished activity compared with activity previously observed in **13**-**15**. We also incorporated a *tert*-butyl group on the pendant benzyl (**17**) to more fully occupy the displaced water pocket. This modification only led to additional molecular weight, with no potency gain compared with **13**. It was surprising that the *para*-methyl benzylic ether substitution (**18**) with no alcohol showed no EGFR activity in cells and a limited effect in A431 cells. However, in the two chordoma cell lines there was a sharp increase in activity. **18** is one of the most potent compounds seen to date with IC_{50} = 330 nM and 310 nM for UCH-1 and UCH-2, respectively. This result is more impressive considering that UCH-2 is typically less sensitive to compound treatment.[11] However, **18** does show some toxicity in WS1 (IC_{50} = 1.1 μM). Removal of the benzyl in **19** had a similar effect to removing the alcohol in **16** with most activity lost, but moderate potency in A431 was still observed (**Table 2**).

We examined compounds **13**-**19** in four additional primary chordoma cell lines and found subsets of compounds with similar activity (**Table 3**). **13**-**15** showed broadly similar activities between IC_{50} = 1-3 μM, and **14** was slightly weaker on UCH-12 at IC_{50} = 9.3 μM. The removal of the alcohol (**16**) resulted in a loss of all anti-proliferative effects across all 4 cell lines (IC_{50} >10 μM). Compound **17** had activities similar to **13**-**15**, but the lack of activity on UCH-2 (IC_{50} > 100 μM), is even more surprising given these results. **18** was still the standout compound with the only submicromolar potency across these 4 additional cell lines (UCH-12 IC_{50} = 800 nM; **Table 3**). The selectivity index was equivalent to lapatinib, but the activity profile was >10-fold in all and >100-fold in some cell lines. Removal of the benzyl (**19**) had a significant effect on EGFR activity in the 4 additional cell lines, with limited anti-proliferative effects (IC_{50} >10 μM) and an increase in toxicity in WS1 cells.

Table 2. Matched pair comparison of benzyloxyanilines

Compound	R^1	R^2	R^3	R^4	EGFR[a] IC$_{50}$ (μM)	A431	UCH-1	UCH-2	WS1
							IC$_{50}$ (μM)[b]		
13	OMe	OMe	OH	A	14	1.6	1.6	2.4	1.4
14	OMe	H	OH	A	14	1.8	0.93	1.4	1.4
15	H	OMe	OH	A	6.3	1.7	0.49	0.68	0.86
16	OMe	OMe	H	A	>20	21	14	21	>100
17	OMe	OMe	OH	B	13	1.8	1.2	>100	1.9
18	OMe	OMe	H	C	>20	1.5	0.33	0.31	1.1
19	OMe	OMe	H	D	>20	3.4	15	15	3.8

[a]ProQinase In-cell assay (n=1), [b](n=3)

We then solved a small molecule crystal structure of **13** in order to explore the conformation of the aniline portion of the molecule and to directly observe the potential internal hydrogen bond between the carbonyl of the amide and the phenolic alcohol. The small molecule crystal structure of **13** was solved as a monoclinic structure with a 27:73 ratio favoring a species without pre-organization to the internal seven membered ring system (**Figure 5**).[21] Under our crystallisation conditions the phenolic alcohol also formed a 2.98 Å hydrogen bond with the chloride ion.

27 : 73
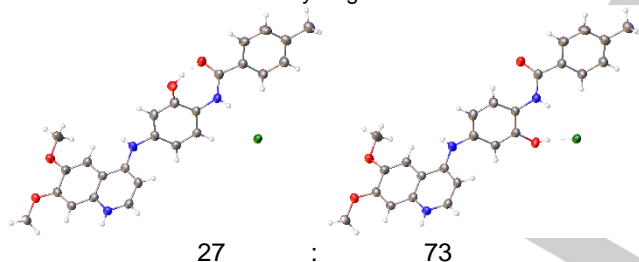
Figure 5. Small molecules crystal structure of **13**

While we would expect the predominant from to be the internally H-bonded structure, with chloride present there is a significant electrostatic component within the lattice acting as an anchor, hindering further pre-organisation. The rigidity imparted by the alcohol onto the pendant arm structure could be leading to the improved potency seen on EGFR with **13** and not observed with **16**.

EGFR inhibitors have been used to target NSCLC, pancreatic cancer, breast cancer, and now chordomas. There is variation in efficacy across inhibitors, with the emergence of secondary resistance to these inhibitors known clinically particularly in the case of NSCLC.[22] We have highlighted a series of modifications, investigating the effect of key structural features and the water network of EGFR on the quin(az)oline scaffold. These modifications can be used to enhance or reduce EGFR activity, and generally have a pronounced effect on cellular potency.

The sensitivity of the kinase ATP water network, while relatively under explored, offers an exciting opportunity to increase potency and potentially increase selectivity.[18-19] One of the key results observed was that removal of one the methoxy groups of **1** led to a significant loss of cellular EGFR potency and anti-proliferative effects. Interestingly, this loss of potency is not observed in the other quinazoline and 3-cyanoquinoline templates, likely due to the orientation of the hinge binder and aniline at a more acute angle in the EGFR ATP binding site (**Figure 2**). This was less significant when looking at the extended aniline structure

Table 3. Investigation of across four patient-derived chordoma cell lines

Cmpd	UCH-1	UCH-2	CH-22	UM-Chor1 IC$_{50}$ (μM)[a]	UCH-12	UCH-7	WS1
Erlotinib[b]	5.1	18	>50	>50	>10	>50	8.6
Gefitinib[b]	1.4	23	>50	>50	>50	>50	23
Lapatinib[b]	3.2	>50	25	25	33	26	13
13	1.6	2.4	1.9	1.5	1.3	1.7	1.4
14	0.93	1.4	1.6	2.6	9.3	1.9	1.4
15	0.49	0.68	1.7	1.7	1.9	1.7	0.86
16	14	21	52	36	73	10	>100
17	1.2	>100	1.7	1.5	2.4	1.9	1.9
18	0.33	0.31	5.8	4.0	0.80	11	1.1
19	15	15	12	21	39	35	3.8

[a](n=3), [b]Literature data reference 13

of **13-16** where the alcohol interaction with Asp855 and conformational rigidity were more significant.[23] The benzyl substitution had an enhanced anti-proliferative effect on chordoma cell line, consistent with the involvement of EGFR as a target for these compounds. This result supports the earlier observation that, despite not being involved in the key hinge binding interactions, the benzyl had a pronounced effect on EGFR activity, likely due to displacement of EGFR active site water molecules.

Conclusions

In summary, two distinct focused series of 4-anilinoquin(az)olines have been identified that interact with the EGFR ATP-binding site water network. The dimethoxy substitution (**1**, **4** & **7**) was shown to have a synergistic effect between the methoxy groups likely due to the occupation of two water binding sites. The second series (**13-17**) utilised conformational rigidity and access to the deeper hydrophobic with the EGFR lipophilic pocket of the ATP binding site. We demonstrated that the alcohol is able to make an interaction both internally and with a key Asp855 (D855) residue within EGFR.

We also identified a potent inhibitor with an acceptable therapeutic window (**18**) of both the A431 NSCLC cells and chordoma cell lines. Benchmarked against literature EGFR inhibitors, **18** has a greater than 10-fold (and in some cases >100-fold) anti-proliferative potency against all chordoma cell lines, with no increase in toxicity profile compared to the representative clinical EGFR inhibitors lapatinib and erlotinib. Chordomas, in particular, are difficult to treat, and **18** along with the other 4-anilinoquin(az)oline series members could yield a clinical candidate with an improved cellular potency and toxicity profile.

Experimental Section

Modelling method

Molecular modelling was performed using Schrödinger Maestro software package (Small-Molecule Drug Discovery Suite 2018-4, Schrödinger, LLC, New York, NY, 2018) Prior to docking simulations structures of small molecules were prepared using and the LigPrep module of Schrodinger suite employing OPLS3e force field.[24] In the case of human EGFR there are numerous PDB structures available representing various ligand binding conformations, showing flexibility in the position of so-called the C-helix. Suitable docking templates were searched using LPDB module of Schrödinger package and carrying out visual inspection of available experimental structures with assistance of LiteMol plug-in available at website of UniProt database. Selected coordinates (PDB:3W2S) have been co-crystallized with at resolution of 1.9 Å with a small molecule inhibitor.[5] The PDB structure of EGFR was H-bond optimized and minimized using standard protein preparation procedure of Schrödinger suite. The ligand docking was performed using SP settings of Schrodinger docking protocol with softened vdw potential (scaling 0.6), except for **7** where induced fit docking protocol was used employing standard settings. In order to improve convergence of docking poses a hydrogen bond constraint to mainchain NH of hinge residue M793 was required, as experimentally observed in the case of quinoline/quinolizine scaffolds. The grid box was centered using coordinate center of the core structure of corresponding x-ray ligand as template. Graphical illustrations were generated using, Maestro, and PyMOL software of Schrödinger.

Hydration Site Analysis

Hydration site analysis calculated with WaterMap (Schrödinger Release 2018-4: WaterMap, Schrödinger, LLC, New York, NY, 2018.). The structure of EGFR (PDB:3W2S) was prepared with Protein Preparation Wizard (as above).[5] Waters

were analyzed within 6 Å from the docked ligand, and the 2 nS simulation was conducted with OPLS3e force field.

Chemistry

General procedure for the synthesis of 4-anilinoquin(az)olines: 4-chloroquin(az)oline derivative (1.0 eq.), aniline derivative (1.1 eq.), and ^iPr₂NEt (2.5 eq.) were suspended in ethanol (10 mL) and refluxed for 18 h. The crude mixture was purified by flash chromatography using EtOAc:hexane followed by 1-5 % methanol in EtOAc; After solvent removal under reduced pressure, the product was obtained as a free flowing solid or recrystallized from ethanol/water.

N-(3-Ethynylphenyl)-6,7-dimethoxyquinolin-4-amine (**1**): light-beige solid (67%, 228 mg, 0.749 mmol) MP 232-234 °C; ^{1}H NMR (400 MHz, DMSO-d_6) δ = 10.94 (s, 1H), 8.35 (d, J=6.9 Hz, 1H), 8.25 (s, 1H), 7.60 (q, J= 1.4 Hz, 1H), 7.58–7.52 (m, 2H), 7.51–7.43 (m, 2H), 6.76 (d, J=6.9 Hz, 1H), 4.34 (s, 1H), 3.99 ppm (d, J=19.4 Hz, 6H); ^{13}C NMR (101 MHz, DMSO-d_6) δ =154.6, 152.9, 149.4, 139.8, 138.1, 135.3, 130.2, 130.0, 128.1, 125.9, 123.2, 111.9, 103.0, 99.7, 99.31, 82.6, 81.9, 56.9, 56.1. HRMS-ESI (m/z): [M+H]$^+$ calcd for $C_{19}H_{16}N_2O_2$ 305.1290, found 305.1278; LC: t_R = 3.75 min, purity > 98%. consistent with previous reports.[15]

N-(3-Ethynylphenyl)-6-methoxyquinolin-4-amine (**2**) yellow solid (67 %, 237 mg, 0.865 mmol) MP 195-197 °C; ^{1}H NMR (400 MHz, DMSO-d_6) δ 11.06 (s, 1H), 8.43 (d, J = 6.8 Hz, 1H), 8.32 (d, J = 2.6 Hz, 1H), 8.06 (d, J = 9.3 Hz, 1H), 7.66 (dd, J = 9.2, 2.6 Hz, 1H), 7.62 (q, J = 1.4 Hz, 1H), 7.59 – 7.54 (m, 2H), 7.54 – 7.47 (m, 1H), 6.83 (d, J = 6.8 Hz, 1H), 4.34 (s, 1H), 4.00 (s, 3H). ^{13}C NMR (101 MHz, DMSO-d_6) δ 158.0, 153.7, 140.6, 137.9, 133.5, 130.3, 130.3, 128.3, 126.0, 125.5, 123.2, 121.9, 118.6, 103.1, 99.8, 82.6, 82.0, 56.6. HRMS m/z [M+H]$^+$ calcd for $C_{18}H_{15}N_2O$: 275.1184 found = 275.1175; LC t_R = 4.46 min, >98% Purity.

N-(3-Ethynylphenyl)-7-methoxyquinolin-4-amine (**3**) mustard solid (69 %, 244 mg, 0.891 mmol) MP 282-284 °C; ^{1}H NMR (400 MHz, DMSO-d_6) δ 11.06 (s, 1H), 8.81 (d, J = 9.4 Hz, 1H), 8.42 (d, J = 7.0 Hz, 1H), 7.62 – 7.57 (m, 1H), 7.57 – 7.52 (m, 2H), 7.52 – 7.43 (m, 2H), 7.40 (dd, J = 9.3, 2.5 Hz, 1H), 6.72 (d, J = 7.0 Hz, 1H), 4.34 (s, 1H), 3.96 (s, 3H). ^{13}C NMR (101 MHz, DMSO-d_6) δ 163.0, 154.3, 142.3, 140.7, 137.8, 130.3 (s, 2C), 128.3, 126.1, 125.8, 123.2, 118.2, 111.6, 99.9, 99.3, 82.6, 82.0, 56.0. HRMS m/z [M+H]$^+$ calcd for $C_{18}H_{15}N_2O$: 275.1184 found = 275.1175; LC t_R = 4.44 min, >98% Purity.

N-(3-Ethynylphenyl)-6,7-dimethoxyquinazolin-4-amine (**4**) colourless solid (74 %, 251 mg, 0.824 mmol) MP 237-239 °C; ^{1}H NMR (500 MHz, DMSO-d_6) δ 11.48 (s, 1H), 8.85 (s, 1H), 8.38 (s, 1H), 7.88 (t, J = 1.8 Hz, 1H), 7.79 (ddd, J = 8.1, 2.2, 1.1 Hz, 1H), 7.49 (t, J = 7.8 Hz, 1H), 7.40 (dt, J = 7.7, 1.3 Hz, 1H), 7.37 (s, 1H), 4.28 (s, 1H), 4.02 (s, 3H), 3.99 (s, 3H). ^{13}C NMR (125 MHz, DMSO-d_6) δ 158.1, 156.3, 150.2, 148.8, 137.4, 136.0, 129.2, 129.2, 127.6, 125.3, 122.0, 107.4, 104.1, 99.9, 82.9, 81.3, 57.0, 56.5. HRMS *m/z* [M+H]$^+$ calcd for $C_{18}H_{16}N_3O_2$: 306.1243, found 306.1230, LC t_R = 3.41 min, >98% Purity.

N-(3-Ethynylphenyl)-6-methoxyquinazolin-4-amine (**5**) yellow solid (56%, 119 mg, 0.432 mmol) MP 176-178 °C; ^{1}H NMR (400 MHz, DMSO-d_6) δ 11.91 (s, 1H), 8.89 (s, 1H), 8.56 (d, J = 2.7 Hz, 1H), 7.96 (d, J = 9.1 Hz, 1H), 7.92 (t, J = 1.8 Hz, 1H), 7.83 (ddd, J = 8.1, 2.2, 1.2 Hz, 1H), 7.73 (dd, J = 9.1, 2.6 Hz, 1H), 7.54 – 7.47 (m, 1H), 7.42 (dt, J = 7.7, 1.3 Hz, 1H), 4.29 (s, 1H), 4.02 (s, 3H). ^{13}C NMR (101 MHz, DMSO-d_6) δ 159.2, 159.0, 148.8, 137.1, 133.5, 129.6, 129.1, 127.8, 127.1, 125.5, 122.0, 121.4, 114.8, 104.8, 82.9, 81.4, 56.9. HRMS m/z [M+H]$^+$ calcd for $C_{17}H_{14}N_3O$: 276.1137 found = 276.1127; LC t_R = 3.47 min, >98% Purity.

N-(3-Ethynylphenyl)-7-methoxyquinazolin-4-amine (**6**) colourless solid (68 %, 241 mg, 0.874 mmol) MP 223-225 °C; ^{1}H

NMR (400 MHz, DMSO-d_6) δ 11.72 (s, 1H), 8.96 (d, J = 9.3 Hz, 1H), 8.91 (s, 1H), 7.89 (t, J = 1.9 Hz, 1H), 7.78 (ddd, J = 8.1, 2.2, 1.2 Hz, 1H), 7.59 – 7.36 (m, 4H), 4.29 (s, 1H), 3.98 (s, 3H). ^{13}C NMR (101 MHz, DMSO-d_6) δ 164.9, 159.2, 150.9, 141.0, 137.1, 129.5, 129.2, 127.7, 127.2, 125.4, 122.0, 107.3, 100.2, 82.9, 81.4, 56.3. HRMS m/z [M+H]$^+$ calcd for $C_{17}H_{14}N_3O$: 276.1137, found 276.1127, LC t_R = 3.34 min, >98% Purity.

4-((3-Ethynylphenyl)amino)-6,7-dimethoxyquinoline-3-carbonitrile (7) beige solid (69 %, 229 mg, 0.694 mmol) MP 241-243 °C; ^{1}H NMR (400 MHz, DMSO-d_6) δ 11.46 – 11.29 (s, 1H), 8.98 (s, 1H), 8.25 (s, 1H), 7.73 – 7.29 (m, 5H), 4.30 (s, 1H), 4.00 (s, 3H), 3.99 (s, 3H). ^{13}C NMR (101 MHz, DMSO-d_6) δ 155.4, 152.6, 150.2, 147.2, 138.0, 130.9, 129.6, 129.0, 126.7, 122.6, 114.2, 113.0, 103.8, 101.4, 86.5, 82.7, 81.8, 56.9, 56.4. HRMS m/z [M+H]$^+$ calcd for $C_{20}H_{16}N_3O_2$: 330.1243 found = 330.1237; LC t_R = 4.70 min, >98% Purity.

4-[(3-Ethynylphenyl)amino]-6-methoxyquinoline-3-carbonitrile (8) yellow solid (58 % 199 mg, 0.663 mmol) MP 245-247 °C; ^{1}H NMR (400 MHz, DMSO-d_6) δ 11.72 (s, 1H), 9.02 (s, 1H), 8.40 (d, J = 2.6 Hz, 1H), 8.10 (d, J = 9.2 Hz, 1H), 7.72 (dd, J = 9.2, 2.6 Hz, 1H), 7.61 (m, 1H), 7.57 - 7.40 (m, 3H), 4.31 (s, 1H), 4.00 (s, 3H). ^{13}C NMR (101 MHz, DMSO-d_6) δ 158.9, 153.7, 147.3, 137.7, 133.8, 131.3, 129.6, 129.3, 127.0, 126.2, 123.3, 122.6, 120.0, 114.1, 104.3, 86.6, 82.7, 81.8, 56.8. HRMS m/z [M+H]$^+$ calcd for $C_{19}H_{14}N_3O$: 300.1137 found = 300.1135; LC t_R = 4.90 min, >98% Purity.

4-[(3-Ethynylphenyl)amino]-7-methoxyquinoline-3-carbonitrile (9) yellow solid (62 %, 212 mg, 0.708 mmol) MP 245-247 °C, ^{1}H NMR (400 MHz, DMSO-d_6) δ 11.67 (s, 1H), 9.06 (s, 1H), 8.88 (d, J = 9.4 Hz, 1H), 7.75 – 7.28 (m, 6H), 4.31 (s, 1H), 3.98 (s, 3H). ^{13}C NMR (101 MHz, DMSO-d_6) δ 164.0, 154.1, 149.8, 141.0, 137.6, 131.3, 129.6, 129.3, 127.1, 126.7, 122.6, 119.0, 114.0, 112.6, 101.7, 86.2, 82.7, 81.8, 56.3. HRMS m/z [M+H]$^+$ calcd for $C_{19}H_{13}N_3O$: 300.1137 found = 300.1130; LC t_R = 4.40 min, >98% Purity.

N-{4-[(6,7-Dimethoxyquinolin-4-yl)amino]-2-hydroxyphenyl}-4-methylbenzamide (13) as a colorless solid (85 %, 151 mg, 0.351 mmol) MP decomposed >280 °C; ^{1}H NMR (400 MHz, DMSO-d_6) δ 10.58 (s, 1H), 10.46 (s, 1H), 9.53 (s, 1H), 8.35 (d, J = 6.9 Hz, 1H), 8.12 (s, 1H), 7.91 (d, J = 8.3 Hz, 2H), 7.44 (s, 1H), 7.35 (d, J = 8.0 Hz, 2H), 7.07 (d, J = 2.4 Hz, 1H), 6.94 (dd, J = 8.5, 2.4 Hz, 1H), 6.77 (d, J = 6.9 Hz, 1H), 3.99 (d, J = 11.8 Hz, 6H), 2.40 (s, 3H). ^{13}C NMR (101 MHz, DMSO-d_6) δ 165.1, 154.6, 153.2, 150.1, 149.4, 141.8, 139.8, 135.3, 134.3, 131.4, 129.1 (s, 2C), 127.6 (s, 2C), 125.1, 124.5, 115.8, 112.8, 111.5, 102.6, 99.9, 99.2, 56.7, 56.2, 21.0. HRMS m/z [M+H]$^+$ calcd for $C_{25}H_{24}N_3O_4$: 430.1767 found = 430.1751; LC t_R = 4.46 min, >98% Purity.

N-(2-Hydroxy-4-((6-methoxyquinolin-4-yl)amino)phenyl)-4-methylbenzamide (14) as a yellow solid (56 %, 89 mg, 0.232 mmol) MP decomposed >280 °C; ^{1}H NMR (500 MHz, DMSO-d_6) δ 10.73 (s, 1H), 10.49 (s, 1H), 9.54 (s, 1H), 8.43 (d, J = 6.8 Hz, 1H), 8.19 (d, J = 2.6 Hz, 1H), 8.01 (d, J = 9.2 Hz, 1H), 7.92 (dd, J = 8.4, 6.8 Hz, 3H), 7.66 (dd, J = 9.3, 2.6 Hz, 1H), 7.35 (d, J = 8.0 Hz, 2H), 7.09 (d, J = 2.4 Hz, 1H), 6.96 (dd, J = 8.5, 2.4 Hz, 1H), 6.84 (d, J = 6.8 Hz, 1H), 3.99 (s, 3H), 2.40 (s, 3H). ^{13}C NMR (126 MHz, DMSO-d_6) δ 165.1, 158.0, 153.8, 150.2, 141.8, 140.7, 134.1, 133.6, 131.4, 129.1 (s, 2C), 127.6 (s, 2C), 125.3, 125.2, 124.6, 122.1, 118.4, 115.8, 112.8, 102.8, 99.6, 56.5, 21.0. HRMS m/z [M+Na]$^+$ calcd for $C_{24}H_{21}N_3O_3Na$: 422.1481 found = 422.1185; LC t_R = 4.23 min, >98% Purity.

N-(2-Hydroxy-4-((7-methoxyquinolin-4-yl)amino)phenyl)-4-methylbenzamide (15) as a yellow solid (67 %, 111 mg, 0.278 mmol) MP decomposed >270 °C; ^{1}H NMR (500 MHz, DMSO-d_6) δ 9.92 (s, 1H), 9.46 (s, 1H), 8.83 (s, 1H), 8.39 (d, J = 5.3 Hz, 1H), 8.28 (d, J = 9.3 Hz, 1H), 8.06 – 7.79 (m, 2H), 7.66 (d, J = 8.5 Hz, 1H), 7.34 (d, J = 8.0 Hz, 2H), 7.25 (d, J = 2.7 Hz, 1H), 7.16 (dd, J = 9.2, 2.7 Hz, 1H), 6.92 (d, J = 2.4 Hz, 1H), 6.87 – 6.67 (m, 2H), 3.90 (s, 3H), 2.39 (s, 3H). ^{13}C NMR (126 MHz, DMSO-d_6) δ 165.1, 159.9, 150.9, 150.8, 150.2, 147.7, 141.6, 138.2, 131.5, 129.0 (s, 2C), 127.5 (s, 2C), 124.9, 123.5, 121.8, 116.5, 114.3, 113.1, 109.9, 107.8, 100.6, 55.3, 21.0. HRMS m/z [M+H]$^+$ calcd for $C_{24}H_{22}N_3O_3$: 400.1661 found = 400.1647; LC t_R = 4.21 min, >98% Purity.

N-(4-((6,7-Dimethoxyquinolin-4-yl)amino)phenyl)-4-methylbenzamide mustard solid (16) 4-chloro-6,7-dimethoxyquinoline (200 mg, 0.89 mmol) and N-(4-aminophenyl)-4-methylbenzamide (222.6 mg, 0.98 mmol) Pd$_2$(dba)$_3$ (122.8 mg, 0.13 mmol), XPhos (64 mg, 0.13 mmol) and caesium carbonate (874 mg, 2.68 mmol) were all suspended in DMF 15 mL and degassed for 5 min. The mixture was held at reflux at 140 °C for 18 h. The crude mixture was then passed through a plug of celite 545 before been purified by flash chromatography 20- 100% EtOAc:hexane followed by 1–5 % methanol/ethyl acetate and solvent removed under reduced pressure to yield the product as a free following solid: (72 %, 266 mg, 0.64 mmol) MP 122-125 °C ^{1}H NMR (400 MHz, DMSO-d_6) δ 10.20 (s, 1H), 8.68 (s, 1H), 8.26 (d, J = 5.3 Hz, 1H), 8.09 – 7.72 (m, 4H), 7.69 (s, 1H), 7.63 – 7.26 (m, 4H), 7.24 (s, 1H), 6.73 (d, J = 5.3 Hz, 1H), 3.92 (d, J = 13.4 Hz, 6H), 2.40 (s, 3H). ^{13}C NMR (101 MHz, DMSO-d_6) δ 165.6, 152.0, 148.6, 148.5, 147.4, 146.1, 141.9, 136.6, 135.7, 132.6, 129.4 (s, 2C), 128.1 (s, 2C), 123.6 (s, 2C), 121.8 (s, 2C), 114.1, 108.6, 101.4, 100.7, 56.4, 55.9, 21.5. HRMS m/z [M+H]$^+$ calcd for $C_{25}H_{24}N_3O3$: 414.1818 found = 414.1808; LC t_R = 5.05 min, >98% Purity.

4-($tert$-Butyl)-N-(4-((6,7-dimethoxyquinolin-4-yl)amino)-2-hydroxyphenyl)benzamide (17) as a bright yellow solid (68 %, 103 mg, 0.218 mmol) MP decomposed >260 °C; ^{1}H NMR (400 MHz, DMSO-d_6) δ 10.62 (s, 1H), 10.49 (s, 1H), 9.53 (s, 1H), 8.34 (d, J = 7.0 Hz, 1H), 8.14 (s, 1H), 7.94 (d, J = 7.2 Hz, 2H), 7.56 (d, J = 8.0 Hz, 1H), 7.45 (s, 1H), 7.08 (s, 1H), 6.94 (d, J = 8.5 Hz, 1H), 6.76 (d, J = 6.8 Hz, 1H), 3.99 (d, J = 14.2 Hz, 6H), 1.32 (s, 9H). ^{13}C NMR (101 MHz, DMSO-d_6) δ 165.1, 154.7, 154.5, 153.2, 150.0, 149.4, 139.7, 135.3, 134.2, 131.5, 127.4 (s, 2C), 125.3 (s, 2C), 125.1, 124.3, 115.8, 112.8, 111.5, 102.7, 99.9, 99.2, 56.7, 56.1, 34.7, 30.9 (s, 3C). HRMS m/z [M+H]$^+$ calcd for $C_{28}H_{30}N_3O_4$: 472.2236 found = 472.2218; LC t_R = 5.15 min, >98% Purity.

6,7-Dimethoxy-N-(4-((4-methylbenzyl)oxy)phenyl)quinolin-4-amine (18) as a light yellow/cyan solid (74 %, 126 mg, 0.315 mmol) MP 158-160 °C; ^{1}H NMR (400 MHz, DMSO-d_6) δ 10.62 (s, 1H), 8.29 (d, J = 7.0 Hz, 1H), 8.15 (s, 1H), 7.45 (s, 1H), 7.37 (dd, J = 8.5, 2.5 Hz, 4H), 7.29 – 7.04 (m, 4H), 6.55 (d, J = 6.9 Hz, 1H), 5.11 (s, 2H), 3.99 (s, 3H), 3.96 (s, 3H), 2.32 (s, 3H). ^{13}C NMR (101 MHz, DMSO-d_6) δ 157.3, 154.5, 153.6, 149.3, 139.8, 137.2, 135.3, 133.8, 130.1, 129.0 (s, 2C), 127.9 (s, 2C), 127.2 (s, 2C), 115.9 (s, 2C), 111.3, 102.7, 99.9, 98.8, 69.5, 56.7, 56.1, 20.8. HRMS m/z [M+H]$^+$ calcd for $C_{25}H_{25}N_2O_3$: 401.1865 found = 401.1849; LC t_R = 5.16 min, >98% Purity.

N-(4-((6,7-Dimethoxyquinolin-4-yl)amino)phenyl)acetamide (19) as a grey solid (77 %, 144 mg, 0.427 mmol) MP decomposed >260 °C HRMS m/z [M+H]$^+$ calcd for $C_{19}H_{20}N_3O_3$: 338.1505 found = 338.1489; LC t_R = 3.09 min, >98% Purity. Consistent with previous report.[25]

Cell Culture Biology Method

Chordoma cell lines UCH-1 and UCH-2 were cultured in 4:1 IMDM:RPMI supplemented with 10 % Fetal Bovine Serum 1 % Penicillin/Streptomycin in gel-coated flasks. WS1 and A-431 cells were cultured in DMEM supplemented with 10 % Fetal Bovine Serum 1 % Penicillin/Streptomycin. UCH-1 and UCH-2 were seeded at 250 cells/well in gel-coated 384 well plates. WS1 cells were seeded at 400 cells/well in 384 well plates, and A-431 cells were seeded at 500 cells/well in 384 well plates. Cells were

treated with compound at 24 h after plating, and cell viability was assessed at 72 h using alamarBlue (ThermoFisher, USA). Fluorescence was measured using Tecan Infinite 200 PRO plate reader with excitation at 535 nM and emission at 590 nM. IC_{50} values were determined by nonlinear regression using Graphpad PrismTM software.
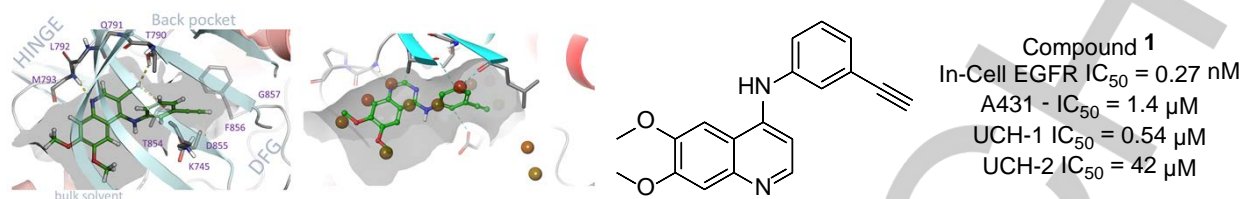
References

[1] Cancer Fact sheet N°297 WHO, **2018**.

[2] (a) Ferguson, F. M.; Gray, N. S. *Nat Rev Drug Discov.* **2018**, *17*, 353-377; (b) http://www.brimr.org/PKI/PKIs.htm

[3] Lynch, T. J.; Bell, D. W.; Sordella, R.; Gurubhagavatula, S.; Okimoto, R. A.; Brannigan, B. W.; Harris, P. L.; Haserlat, S. M.; Supko, J. G.; Haluska, F. G.; Louis, D. N.; Christiani, D. C.; Settleman, J.; Haber, D. A. *N. Engl. J. Med.* **2004**, *350*, 2129-2139.

[4] Maemondo, M.; Inoue, A.; Kobayashi, K.; Sugawara, S.; Oizumi, S.; Isobe, H.; Gemma, A.; Harada, M.; Yoshizawa, H.; Kinoshita, I.; Fujita, Y.; Okinaga, S.; Hirano, H.; Yoshimori, K.; Harada, T.; Ogura, T.; Ando, M.; Miyazawa, H.; Tanaka, T.; Saijo, Y.; Hagiwara, K.; Morita, S.; Nukiwa, T. *N. Engl. J. Med.* **2010**, *362*, 2380-2388.

[5] Wood, E. R.; Truesdale, A. T.; McDonald, O. B.; Yuan, D.; Hassell, A.; Dickerson, S. H.; Ellis, B.; Pennisi, C.; Horne, E.; Lackey, K.; Alligood, K. J.; Rusnak, D. W.; Gilmer, T. M.; Shewchuk, L. *Cancer Res.* **2004**, *64*, 6652-6659.

[6] Sigismund, S.; Avanzato, D.; Lanzetti, L. *Mol Oncol.* **2018**, *12*, 3-20.

[7] George, B.; Bresson, D.; Herman, P.; Froelich, S. *Neurosurg Clin N Am.* **2015**, *26*, 437-452.

[8] Ferraresi, V.; Nuzzo, C.; Zoccali, C.; Marandino, F.; Vidiri, A.; Salducca, N.; Zeuli, M.; Giannarelli, D.; Cognetti, F.; Biagini, R. *BMC Cancer.* **2010**, *28*, 22.

[9] Akhavan-Sigari, R.; Gaab, M.; Rohde, V.; Abili, M.; Ostertag, H. *Anticancer Res.* **2014**, *34*, 623-630.

[10] Magnaghi, P.; Salom. B.; Cozzi, L.; Amboldi, N.; Ballinari, D.; Tamborini, E.; Gasparri, F.; Montagnoli, A.; Raddrizzani, L.; Somaschini, A.; Bosotti, R.; Orrenius, C.; Bozzi, F.; Pilotti, S.; Galvani, A.; Sommer, J.; Stacchiotti, S.; Isacchi, A. *Mol Cancer Ther.* **2018**, *17*, 603-613.

[11] Scheipl, S.; Barnard, M.; Cottone, L.; Jorgensen, M.; Drewry, D. H.; Zuercher, W. J.; Turlais, F.; Ye, H.; Leite, A. P.; Smith, J. A.; Leithner, A.; Möller, P.; Brüderlein, S.; Guppy, N.; Amary, F.; Tirabosco, R.; Strauss, S. J.; Pillay, N.; Flanagan, A. M. *J Pathol.* **2016**, *239*, 320-334.

[12] Magnaghi, P.; Salom, B.; Cozzi, L.; Amboldi, N.; Ballinari, D.; Tamborini, E.; Gasparri, F.; Montagnoli, A.; Raddrizzani, L.; Somaschini, A.; Bosotti, R.; Orrenius, C.; Bozzi, F.; Pilotti, S.; Galvani, A.; Sommer, J.; Stacchiotti, S.; Isacchi, A. *Mol Cancer Ther.* **2018**, *17*, 603-613.

[13] Asquith, C. R. M.; Naegeli, K. M.; East, M. P.; Laitinen, T.; Havener, T. M.; Wells, C. I.; Johnson, G. L.; Drewry, D. H.; Zuercher, W. J.; Morris, D. C. *J Med Chem.* **2019**, *62*, 4772-4778.

[14] Knight, Z. A.; Shokat, K. M. *Chem Biol.* **2005**, *12*, 621-637.

[15] Asquith, C. R. M.; Laitinen, T.; Bennett, J. M.; Godoi, P. H.; East, M. P.; Tizzard, G. J.; Graves, L. M.; Johnson, G. L.; Dornsife, R. E.; Wells, C. I.; Elkins, J. M.; Willson, T. M.; Zuercher, W. J. *ChemMedChem* **2018**, *13*, 48-66.

[16] Asquith, C. R. M.; Berger, B. T.; Wan, J.; Bennett, J. M.; Capuzzi, S. J.; Crona, D. J.; Drewry, D. H.; East, M. P.; Elkins, J. M.; Fedorov, O.; Godoi, P. H.; Hunter, D. M.; Knapp, S.; Müller, S.; Torrice, C. D.; Wells, C. I.; Earp, H. S.; Willson, T. M.; Zuercher, W. J. *J. Med. Chem.* **2019**, *62*, 2830-2836.

[17] Fabian, M. A.; Biggs, W. H., 3rd; Treiber, D. K.; Atteridge, C. E.; Azimioara, M. D.; Benedetti, M. G.; Carter, T. A.; Ciceri, P.; Edeen, P. T.; Floyd, M.; Ford, J. M.; Galvin, M.; Gerlach, J. L.; Grotzfeld, R. M.; Herrgard, S.; Insko, D. E.; Insko, M. A.; Lai, A. G.; Lelias, J. M.; Mehta, S. A.; Milanov, Z. V.; Velasco, A. M.; Wodicka, L. M.; Patel, H. K.; Zarrinkar, P. P.; Lockhart, D. J. *Nat Biotechnol* **2005**, *23*, 329-336.

[18] Cappel, D.; Sherman, W.; Beuming, T. *Curr Top Med Chem.* **2017**, *17*, 2586-2598.

[19] Robinson, D. D.; Sherman, W.; Farid, R. *ChemMedChem.* **2010**, *5*, 618-627.

[20] Schrödinger suite 2015-3: Maestro, version 10.3; Ligprep, version 2.8; QM-Polarized Ligand Docking; Glide version 6.8, Jaguar version 8.9, QSite version 6.8, Schrödinger, LLC, New York, NY, 2015)

[21] Compound **13** - CCDC number 1894101

[22] Sogabe, S.; Kawakita, Y.; Igaki, S.; Iwata, H.; Miki, H.; Cary, D. R.; Takagi, T.; Takagi, S.; Ohta, Y.; Ishikawa, T. *ACS Med Chem Lett.* **2012**, *4*, 201-205.

[23] Dixit, A.; Verkhivker, G. M. *Comput Math Methods Med.* **2014**, *2014*, 653487.

[24] Harder, E.; Damm, W.; Maple, J.; Wu, C.; Reboul, M.; Xiang, J. Y.; Wang, L.; Lupyan, D.; Dahlgren, M. K.; Knight, J. L.; Kaus, J. W.; Cerutti, D. S.; Krilov, G.; Jorgensen, W. L.; Abel, R.; Friesner, R. A. *J Chem Theory Comput.* **2016**, *12*, 281-296.

[25] Kubo, K.; Shimizu, T.; Ohyama, S.; Murooka, H.; Iwai, A.; Nakamura, K.; Hasegawa, K.; Kobayashi, Y.; Takahashi, N.; Takahashi, K.; Kato, S.; Izawa, T.; Isoe, T. *J Med Chem.* **2005**, *48*, 1359-1366.

Entry for the Table of Contents

Insert graphic for Table of Contents here.

Compound **1**
In-Cell EGFR IC_{50} = 0.27 nM
A431 - IC_{50} = 1.4 µM
UCH-1 IC_{50} = 0.54 µM
UCH-2 IC_{50} = 42 µM

Preparation of a series of structurally focused modular arrays of quin(az)oline-based inhibitors of the epidermal growth factor receptor (EGFR) were investigated against non-small cell lung cancer and chordomas with the identification of potent relatively non-toxic compounds. Several key structural features including an interaction with the EGFR ATP binding site were probed, along with the specific targeting of the active site water network.